Cement and Concrete Research 40 (2010) 352–358

Contents lists available at ScienceDirect

Cement and Concrete Research

journal homepage: http://ees.elsevier.com/CEMCON/default.asp

High porosity (>90%) cementitious foams

F.K. Akthar, J.R.G. Evans *

Department of Chemistry, University College London, 20 Gordon Street, London, WC1H 0AJ, United Kingdom

ARTICLE INFO

Article history:
Received 7 July 2009
Accepted 12 October 2009

Keywords:
B. Microstructure
C. Compressive strength
C. Transport properties
E. fibre reinforcement
Foams

ABSTRACT

High porosity foams based on Portland limestone cement or gypsum plaster were prepared by a simple method of stirring and drying using low levels of the food additives: methyl cellulose and iota carageenan gum. Thermal conductivity of 0.11 $W m^{-1} K^{-1}$ at 92% porosity was achieved but compressive strength was also very low. Foams were almost closed cell. Attempts to improve strength by incorporation of short staple glass fibre were only partially successful because of a change in the failure mode from progressive collapse to uniform fibre-cement debonding facilitated by the ability of the fibre network to transmit stress throughout the assembly. This approach to fire resistant insulation materials does not yet match the high strength/conductivity ratios of calcium silicate products but deserves exploring because of the simplicity of preparation and the compositional freedom for using mixtures of hydraulic cement and other powders.

1. Introduction

There are now many methods of making foams from metals and ceramics in which the material is initially in powder form. They include the use of porosifiers [1], organic gels [2], replication on a pre-existing polymer foam template [3] foaming polymer vehicles [4,5] and aqueous foaming agents [6]. The method used here is similar to that proposed for high temperature ceramic foams except that hydraulic cement powder or gypsum plaster are used and indeed, in principle it can be applied to any cementitious powder or mixture of powders. This work is motivated by the requirement for low cost, fire resistant thermal insulation materials in which the general aim is to obtain high porosity but to retain high ratios of strength to thermal conductivity. Rules for the porosity-dependence of thermal insulation materials have been collated [7] and since the thermal conductivity of air is 0.026 $W m^{-1} K^{-1}$ high porosity is sought but pore size should be lower than 4 mm to inhibit convective heat transfer and cells should preferably be closed or nearly so. This means the cell gas can be regarded as having the thermal conductivity of still air. For porous solids in general, it is only if the pore size is in the nanometer regime, as is the case for aerogels and possibly for the gel porosity fraction in cement pastes, that it is possible to reduce the effective thermal conductivity of the gas phase in an unsealed product because Knudsen conditions prevail [8].

Cement and concrete foams can be made by adding aluminium powder to the mix before adding gauging water or injecting aqueous foam into the cement slurry to give foams with porosity 50–90%. Tonyan and Gibson [9] prepared foams with densities of 160–1600 kg m^{-3} by injecting a preformed foam generated by compressed air into a cement slurry and then mixing with a food mixer. Microsilica and a plasticiser were added to the cement–water slurry and polyester fibres were incorporated to improve foam stability and strength. The compressive strength σ expressed in terms of density ρ, theoretical density ρ_s and porosity p, approximately followed a relationship which is suitable for application at very high porosity levels:

$$\sigma = \sigma_{fs}\left(\frac{\rho}{\rho_s}\right)^{1.2}\exp^{-4.6p} \quad (1)$$

where σ_{fs} is the modulus of rupture of the cell wall material. Examples of actual strength values in the low density region were: 160 kg m^{-3}: 0.04 MPa and 224 kg m^{-3}: 0.12 MPa. The estimated value of the MoR of the cell wall σ_{fs}, was 6.1 MPa. Karam and Tonyan [10] note that the pores follow a fractal distribution over a range of sizes. Indeed surfactants are added to concrete to entrain air voids which will relieve pressure and hence damage due to freeze–thaw conditions during setting [11]. Attempts have been made to improve the properties of cement foams, for example, reinforcement with polyurethane to give up to 60 wt.% cement and a density of 350 kg m^{-3} develops compressive strengths in the region of 2 MPa [12]. Polyvinyl alcohol fibres [13] or polystyrene beads [14] have been added. The latter approach retains compressive strength at greatly reduced density thus almost doubling the strength/density ratio. A more complex system designed as a foam core for sandwich panels is based on additions of glass micro-balloons, styrene-butadiene rubber latex, glass fibre and nanoclay [15].

We sought to extend the foaming method previously reported for high temperature ceramics [6] to explore its generality to hydraulic

* Corresponding author. Tel.: +44 207679 4689; fax: +44 207679 4603.
E-mail address: j.r.g.evans@ucl.ac.uk (J.R.G. Evans).

0008-8846/$ – see front matter © 2009 Elsevier Ltd. All rights reserved.
doi:10.1016/j.cemconres.2009.10.012

setting fine powders of almost any type recognising that the ability to reach very high levels of porosity may not confer adequate mechanical strength for immediate application. The method is based on a combination of additives used in the food industry. Short staple glass fibre was added in an attempt to recover compressive strength by creating a three dimensional interpenetrating structure of well-bonded fibres in which each fibre was capable of bridging several pores in the millimetre size range.

2. Experimental details

The materials and their sources are listed in Table 1. The development of formulation was mainly based on preparation of mixtures of distilled water and Portland limestone cement (PLC) of volume 200 ml with additions of methyl cellulose (MC) and iota carageenan gum (iCG) systematically varied. The foam was produced by an electrical whisk operated for approximately 120 s in a graduated vessel and the foam ratio (foam volume/initial volume) was recorded after which the foam was cast into rectangular moulds of 30 mm depth and left to cure and for excess water to dry at ambient conditions. The glass fibre was alkali-resistant, 18 μm diameter filament in the form of 6 mm chopped rovings. It was added either as-received or after dispersion for 600 s in propan-2-ol using an ultrasonic probe (U200S, IKA Labortechnik, Germany) and drying, the fibres being introduced into the suspension in stages during foaming to facilitate mixing. The same procedure was followed for the plaster foams. Systematic variation in composition was used to find the minimum water content and the minimum organic constituents and still retain high air entrapment.

A Hitachi S-3400N Scanning Electron Microscope (SEM) operating at 5 kV was used to examine the foams after hydration for 5.2 Ms (60 days). Fracture surfaces were sputter coated with gold. Compression testing was done on a HSKS Hounsfield mechanical testing machine fitted with a 250 N load cell. A Bruker AXS D8 Discover X-ray diffractometer using partially monochromatic, CuKα radiation operating at a voltage of 40 kV and current of 40 mA was used to examine the foam prepared with 13.5 vol.% PLC ($w/c=2$) at a scanning speed of 5° of 2θ/min in the range of 0–65° of 2θ.

Thermal conductivity was measured using the hot-wire (parallel) method according to the European Standard [16]. This method is suitable for thermal conductivities less than 25 $W m^{-1} K^{-1}$ and requires the determination of the temperature increase as a function of time at a distance of 15 mm from a linear heat source (hot-wire) that is sandwiched between two foams slabs of $200\times100\times50\pm1$ mm^3. In order to have confidence in the method, measurements were also made on blocks of expanded polystyrene of porosity 99% for which the thermal conductivity can be calculated [7].

Table 1
Details of the materials used for the porous cement making process.

Material	Sources information
Portland limestone cement	Mastercrete original cement. Portland limestone cement, density original powder* 3200 kg m^{-3} after hydration*: 2514 kg m^{-3}
Glass fibre	Cem-FIL^{tm} Go/3 alkali-resistant chopped strand 6 mm staple. Saint-Gobain Vetrotex (UK) LTD, 2580 kg m^{-3}
Plaster	One coat plaster. Lightweight gypsum building material plaster, Knaufdrywall–Sittingbourne, 2695 kg m^{-3}; hydrated 2320 kg m^{-1}.
Methyl cellulose (MC)	Methocel food grade, product type: A4CFG(E461), Dow Methocel Food Group, Europe.
Iota carageenan (iCG)	Gelcarin GP 379 FMC Biopolymer, Bournel, Belgium.

*Density bottle using propan-2-ol.

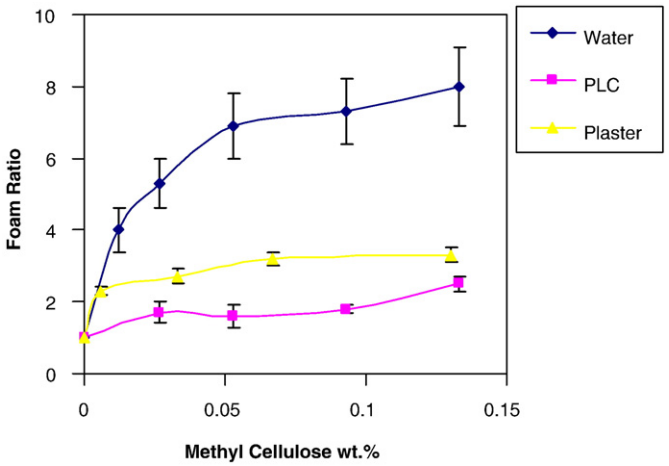

Fig. 1. Foam ratio as a function of methyl cellulose content (wt.% based on water). Water/cement ratio by mass = 1 giving 24 vol.% cement; water/plaster ratio = 1.3 giving 22 vol.% plaster.

3. Results and discussion

3.1. Portland limestone cement foams

Fig. 1 shows the dependence of foam ratio on MC addition for a fixed PLC content of 24 vol.% (plotting data for samples 5–9 with $w/c=1$ in Table 2) and compares it with the foam ratio for water only. Throughout this work, the MC content was based on the mass of powder, PLC or plaster, but for the purpose of this comparison, the masses of PLC and water were the same (Table 2) so that the MC content for the PLC curve, the water curve and the plaster curve are directly comparable, all reflecting the aqueous concentration. Clearly the addition of powder reduces the foam ratio significantly compared with water but the trend with MC content is the same. The curve for water provides more discrimination and justifies the level of 0.13 wt.% MC based on PLC which was used in much subsequent work, a choice based upon the wish to increase foam ratio with minimum addition of organic additive. Converted to volume fraction, the PLC powder occupied 24 vol.% of the suspension, slightly higher than that used for the plaster foam (22 vol.%) and in subsequent work, a lower fraction was used (It is the convention to express composition in w/c ratio but the behaviour of suspensions is often dependent on solids volume fraction and less dependent on solids density and so both designations are used here). If MC was eliminated as in sample 9 (Table 2), any foam that did develop during stirring quickly collapsed, confirming its role as a foaming agent.

The results of the preliminary samples 1 and 2 (Table 2) confirm that PLC volume fraction has a significant effect on foam ratio but this is reduced by only 10% from 3.3 to 3.0 when the cement volume fraction rises from 13.5 to 19% (w/c falls from 2.0 to 1.33). Systematic variation of the cement fraction (Fig. 2), plotting data for samples 10 to 14 (Table 2) shows that foam ratio increases as the powder content decreases, levelling off at 13.5 vol.% powder ($w/c=2$). Reducing the water content facilitates drying of excess water and it can be argued that reducing the organic content causes less interference with cement hydration and development of strength. Cellulose ethers are known to retard hydration [17,18]. Density measurements on the cured and dried foam showed that as the powder content in the slurry was increased from 11 vol.% to 32 vol.% (w/c from 2.7 to 0.67), the porosity in the final foam decreased from 94 to 79%.

It was also apparent that a foam could still be obtained if iCG was omitted (Sample 3 in Table 2). However when iCG was eliminated, the foam survived for only about 300 s before collapsing through drainage. The iCG therefore, while not acting as a foaming agent itself, enhanced stability of the organic gel and it was concluded from adjustments of iCG content that a minimum of 0.07 wt.% iCG based on

Table 2
Composition and porosity of PLC foams.

No.	PLC/wt.%	*w/c* by mass	iCG*/wt.%	MC*/wt.%	PLC/vol.%	Foam ratio	Foam+ density/kg m^{-3}	Final porosity %	Porosity Eq. (2)
1	33	2.0	0.13	0.13	13.5	3.3 ± 0.4	220 ± 30	91	95
2	43	1.33	0.13	0.13	19.0	3.0 ± 0.4	250 ± 50	90	92
3	43	1.33	0.0	0.067	19.0	2.5 ± 0.2	230 ± 20	91	90
4	43	1.33	0.13	0.013	19.0	2.4 ± 0.2	–	–	90
5	50	1.0	0.13	0.13	23.8	2.5 ± 0.2	320 ± 30	87	88
6	50	1.0	0.13	0.093	23.8	1.8 ± 0.1	610 ± 20	76	83
7	50	1.0	0.13	0.053	23.8	1.6 ± 0.3	630 ± 40	75	81
8	50	1.0	0.13	0.027	23.8	1.7 ± 0.3	–	–	82
9	50	1.0	0.13	0.0	23.8	1.0	–	–	70
10	27	2.70	0.13	0.13	10.5	3.5 ± 0.5	140 ± 30	94	96
11	33	2.0	0.13	0.13	13.5	3.3 ± 0.4	250 ± 30	90	95
12	43	1.33	0.13	0.13	19.0	2.9 ± 0.3	320 ± 50	87	92
13	50	1.0	0.13	0.13	23.8	2.5 ± 0.2	320 ± 30	87	88
14	60	0.67	0.13	0.13	31.9	2.0 ± 0.2	520 ± 40	79	80

*Based on mass of PLC; +for cured and dried foam.

cement powder was needed to maintain stable foam; slightly higher additions were generally made.

The final porosity P, of the hydrated and dried foam is given approximately by:

$$P \approx 1 - \frac{V_c \rho_p}{F \rho_h} \quad (2)$$

where V_c is the volume fraction of cement powder in the unfoamed suspension, F is the foam ratio, ρ_p (3200 kg m^{-1}) and ρ_h (2514 kg m^{-1}) are the cement powder and hydration densities respectively and were measured in a density bottle with propan-2-ol on the as-received cement and powdered hydrated foam paste. This expression makes it possible to assess how the foam structure sustains itself during drying. Thus for the cement foams, the porosity calculated from Eq. (2) (last col., Table 2) was only slightly higher than the porosity found from density measurement on the hydrated and dried foam (penultimate col., Table 2). This means there had been very little collapse during drying. When applied to the plaster foams using densities in Table 1, the situation was slightly less favourable; there was a deficit of 5% or more when the porosity obtained from density was compared with P from Eq. (1); the organic gel formed by the MC and iCG with calcium sulphate is apparently less robust than the Portland limestone cement suspension and some collapse occurs on drying.

There were some large pores of 3–4 mm not shown in the microscopic images and the foam threw a thin dark sediment, possibly of coarser powder. Fig. 3a shows a general area of the fracture surface with pores in the sub-millimetre region; the pores average (0.70 ±

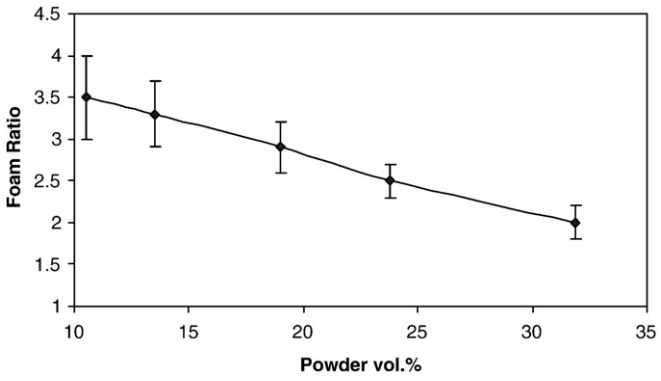

Fig. 2. Foam ratio as a function PLC powder fraction (methyl cellulose and carageenan both at 0.13% based on cement).

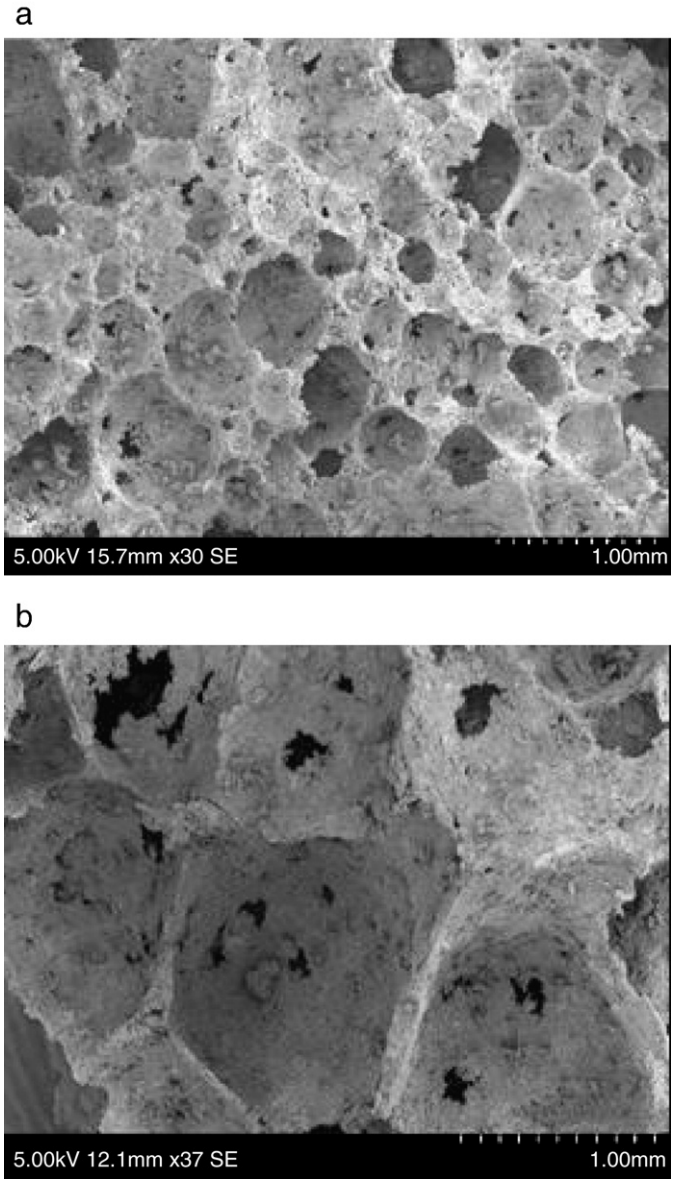

Fig. 3. Scanning electron microscope images (a) 91% porous foam made with 13.5 vol.% cement ($w/c = 2$), (b) higher magnification image showing that the foam is almost closed cell.

0.10) mm in diameter. This foam has a porosity of 91%. Fig. 3b shows a higher magnification image in which the cell windows can be seen as irregular perforations and the strut fracture faces are visible. Generally, as the pore volume fraction of a ceramic foam increases, the structure progresses from closed cell to reticulated as windows (perforations between cells) form and widen. The important observation is that even with the porosity above 90%, the foam is almost entirely closed cell. Fig. 3b shows that there are some small windows beginning to develop but they are not large enough to allow significant convection between cells or significant radiation transfer. With other foaming methods for ceramic materials, it is often the case that reticulated structures develop above about 80% porosity [19]. The XRD trace at 10.4 Ms (120 days) did not differ greatly from the literature trace for an ordinary Portland cement after 15.6 Ms (180 days) [20]; the differences in XRD between OPC and PLC are discussed in more detail by Voglis [21].

The fracture faces of foams reinforced with undispersed and dispersed fibres are shown in Fig. 4a and b respectively. The hydrated cement adheres well to the fibre. The undispersed chopped fibre can be seen still aligned in the original tows whereas the dispersed fibre produces a more chaotic arrangement. Upon addition of glass fibre, the foam ratio was considerably reduced compared to the foam ratio without addition of glass fibre. The effect was less pronounced in the case of undispersed fibres and can be attributed to entanglement effects among fibres that have been freed from their tows opposing the incorporation of air into the liquid. The change in foam ratio brought about by dispersed and undispersed fibre is shown in Fig. 5 in which data for samples G1 to G10 are plotted (Table 3). A similar trend was observed for the plaster foams. It was concluded that as a guide, no more than 15–20 vol.% fibre based on the cement powder should be used. The volume fraction of fibre based on cement is much higher than that used in, for example, concrete where volume fractions in the region 0.1 vol.% provide local reinforcement [22] but in these porous structures the fibres occupy typically less than 2% of available space.

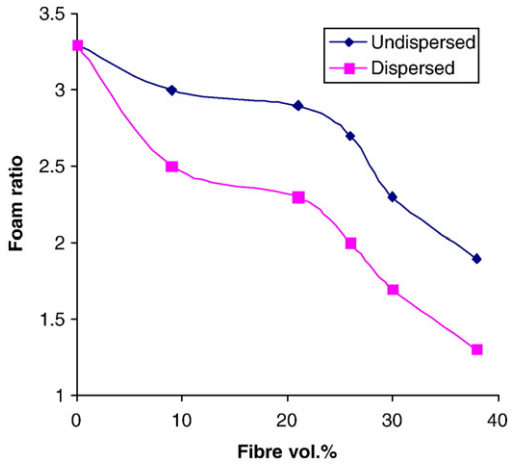

Fig. 5. The effect of undispersed (upper curve) and dispersed (lower curve) short staple glass fibre on foam ratio of cement foams with $w/c = 2$ and 0.7 wt.% iCG, 1.3 wt.% MC based on cement.

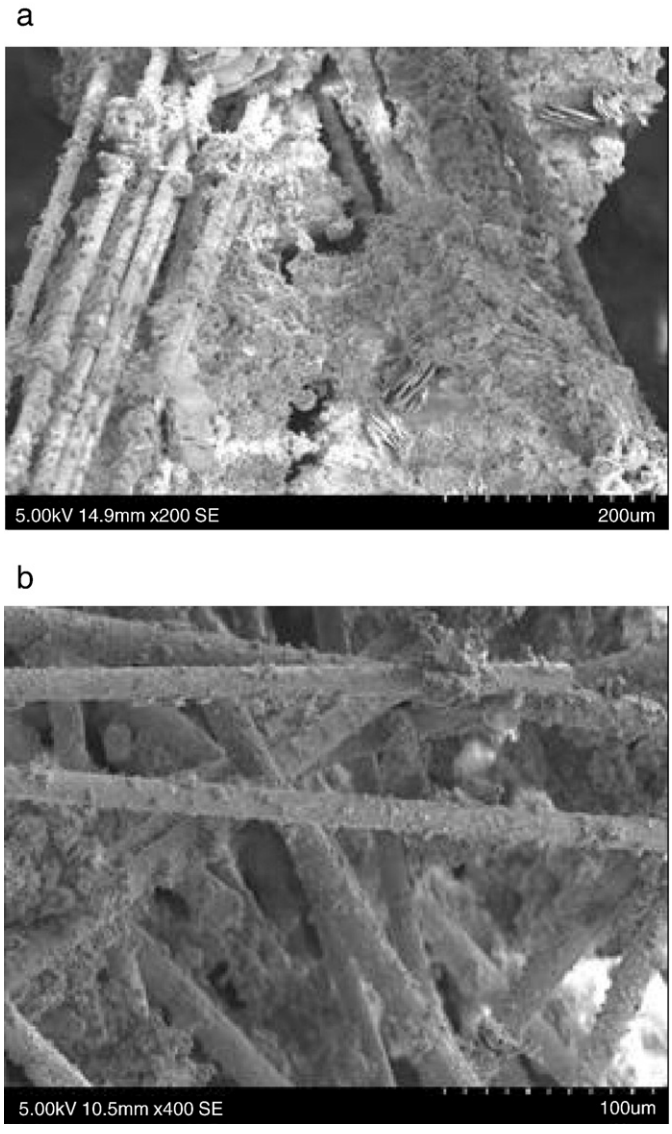

Fig. 4. Fracture face of a cement foam reinforced with 8% fibre; (a) undispersed fibre showing most of the tows intact, (b) dispersed fibre.

3.2. Gypsum plaster foams

Fig. 1 shows the effect of MC content for plaster slurries with 22 vol.% powder, slightly below the volume loading for cement which was 24 vol%. Slightly higher foam ratios are obtained because of the sensitivity to powder volume fraction. The amounts of iCG and MC selected for use in the plaster foam experiments were 0.044 wt.% and 0.089 wt.% respectively based on plaster. A water/plaster weight ratio of 1.3 was sufficient to give a foam ratio of almost 3 and to develop a porosity of 80–85%. Fig. 6 shows the microstructure of the plaster foams; it is similar to the

Table 3
Formulation of Portland limestone cement foams with short staple glass fibre additions.

No.	Fibre vol.%*	Foam ratio	Foam density /kg m^{-3}	Final porosity %
G1	8U	3.0 ± 0.2	220 ± 30	91
G2	18 U	2.9 ± 0.2	230 ± 30	91
G3	25 U	2.7 ± 0.2	240 ± 40	91
G4	33U	2.3 ± 0.2	240 ± 40	91
G5	54 U	1.9 ± 0.2	260 ± 20	90
G6	8D	2.5 ± 0.2	290 ± 20	88
G7	18 D	2.3 ± 0.2	320 ± 40	87
G8	25 D	2.0 ± 0.1	330 ± 50	87
G9	33 D	1.7 ± 0.1	340 ± 60	87
G10	54 D	1.3 ± 0.1	750 ± 10	71

All foams use 13.5 vol.% based on water–cement ($w/c = 2$) and 0.067 wt.% iCG and 0.13 wt.% MC based on PLC.
*Fibre vol.% based on fibre + hydrated PLC; U; undispersed , D; dispersed.

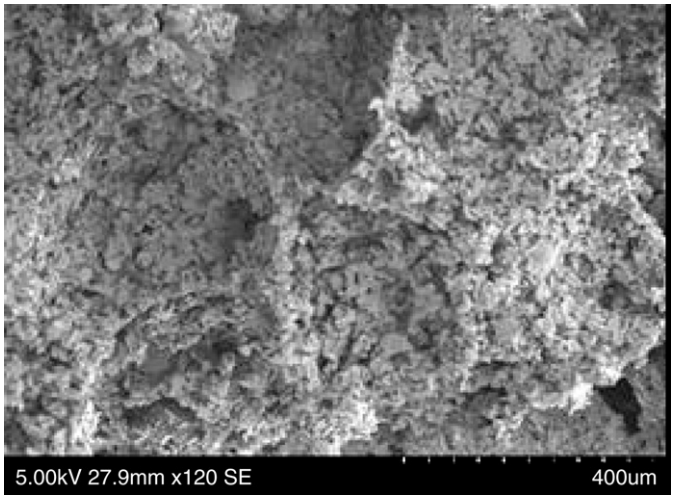

Fig. 6. Scanning electron micrograph of a plaster foam made with a water/plaster ratio = 1.3 by mass and 0.09 wt.% MC and 0.04 wt.% iCG based on plaster.

cement foams with most of the pore diameters in the 0.5–1 mm region and with some larger pores. Fig. 7 shows that the effect on foam ratio of addition of short staple glass fibre to plaster foams is less than the effect on cement foams; again pre-dispersal of the fibre reduces the foam ratio (Table 4) but has less effect on porosity.

3.3. Mechanical testing

The form of the load-deflection curves for the unreinforced foams was similar to that shown by Gibson and Ashby ref. [23, p.177, Fig. 5.1c] for an elastic–brittle foam. The load first rises, representing the initial stage of cell wall bending, followed by a collapse plateau associated with progressive failure of struts throughout the bulk at nominally constant load and then ascending load as the debris is densified. Crushing strength, in the case of such foams, is deduced from average load at the collapse plateau.

Three factors affect the mechanical strength of these foams: (1) The intrinsic strength of the cement cell walls; the foaming method may interfere with hydration reactions through the presence of organic additives. (2) The porosity, which influences strength through the Ashby equation:

$$\sigma = 0.2\sigma_{fs}(\rho^*/\rho_s)^{3/2} \quad (3)$$

(3) The addition of glass fibre may change both foaming and strength. The former effect is shown in Figs. 5 and 7 but the mechanical response of the fibre-reinforced foams was also quite different to that shown by the unreinforced foams. The collapse plateau, although it occurred at similar compressive stress, was drastically shortened and represented only by a 'knee' in the curve. At this point, the foam failed throughout the bulk as the fibres transmitted load through the slab and the cement foam around the fibres failed concurrently. Thereafter the load continued to rise because the network of fibres, still loosely connected by cement structures, supported increasing load but this really represents the densification of debris in the final stage and the foam has already failed.

Fig. 8 shows the dependence of crushing strength on relative density to the power 3/2 for the cement foam in an attempt to gain the straight line predicted by Eq. (3). The failure strength σ_{fs} was extracted from the equation of the line to give $\sigma_{fs} = 8.9$ MPa, slightly higher than the value found by Tonyan and Gibson [9] of 6.1 MPa for Portland cement but their value is deduced from a slightly different equation (Eq. (1)) which includes an exponential function of porosity. This represents the notional flexural strength of cement cell walls and struts and may be distinguished from a flexural strength measurement on a bulk cement paste. It can be seen that all the foam strengths were below 1 MPa. The reinforced foams produced a very short plateau at a slightly lower stress after which the stress continued to rise. The plaster foams had lower crushing strengths in the region 0.04 MPa.

Table 4
Formulations of gypsum plaster foams with short staple glass fibre additions.

No.	Fibre* vol.%	Foam ratio	Foam density /kg m^{-3}	Final porosity %
GP1	12 U	2.8 ± 0.2	530 ± 40	77
GP2	24 U	2.5 ± 0.2	520 ± 40	78
GP3	33 U	2.3 ± 0.2	520 ± 20	78
GP4	43 U	1.7 ± 0.2	550 ± 30	77
GP5	51 U	1.5 ± 0.1	530 ± 30	78
GP6	12 D	2.5 ± 0.2	–	–
GP7	24 D	2.4 ± 0.2	380 ± 60	84
GP8	33 D	2.1 ± 0.2	340 ± 20	86
GP9	43 D	1.3 ± 0.2	340 ± 40	86
GP10	51 D	1.2 ± 0.2	630 ± 40	74

*Fibre vol.% based on fibre + hydrated plaster; U; undispersed , D; dispersed.

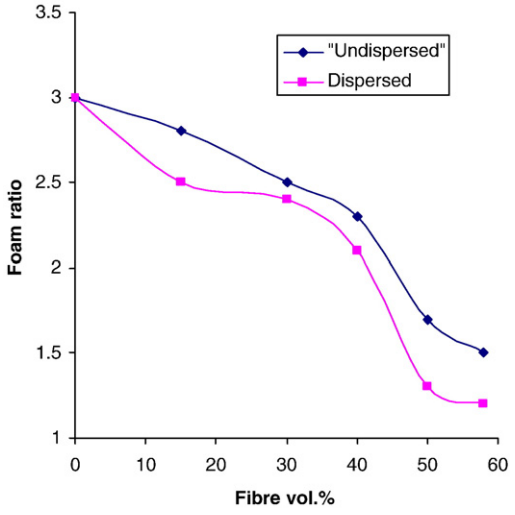

Fig. 7. The effect of dispersed and undispersed glass fibre on foam ratio in plaster foams with a water/plaster ratio = 1.3 by mass.

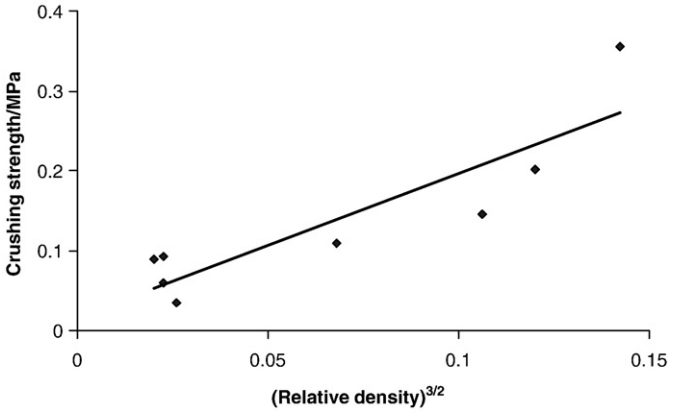

Fig. 8. Gibson–Ashby plot for unreinforced cement foams with 0.13 wt.% MC and 0.13 wt.% iCG.

3.4. Thermal conductivity

The hot-wire (parallel) standard method (BS EN 993-15-1998) has the great advantage of simplicity and has been assessed in conjunction with two guarded hot-plate methods and a steady state radial heat flow method using xonotlite test materials of porosity 92% and 89% [24]. The thermal conductivity of expanded polystyrene blocks of density 7.0 $kg\,m^{-3}$ which corresponds to a porosity of 99.3% (bulk density 1050 $kg\,m^{-3}$) was measured in order to be confident of the method. The value recorded between 20 and 40 °C was $0.031 \pm 0.009\ W\,m^{-1}K^{-1}$. Taking the solid conductivity (k_s) for polystyrene of $0.155\ W\,m^{-1}K^{-1}$ [25] and thermal conductivity of air at 20 °C (k_g) of $0.026\ W\,m^{-1}K^{-1}$, Eq. (2) from reference [7] gives a predicted thermal conductivity for this foam of $0.027\ W\,m^{-1}K^{-1}$ a 12% deviation from that measured. Such variations are typical for thermal conductivity of low conductivity materials [24].

Thermal conductivity of the cement foam was measured on two pairs of blocks 200 mm × 150 mm × 50 mm. For density 193 $kg\,m^{-3}$ (porosity 92%) the conductivity was $0.110 \pm 0.017\ W\,m^{-1}K^{-1}$ and for density 220 $kg\,m^{-1}$ (91% porosity) was $0.135 \pm 0.048\ W\,m^{-1}K^{-1}$.

The apparent thermal conductivity of the cement foam k, can be related to volume fraction of gas by any of a family of semi-empirical equations [7]. A relationship that provides a mid-range estimate was chosen:

$$k = k_s(1-A) + k_g A \quad \text{where } A = \frac{2^n}{2^n - 1}\left(1 - \frac{1}{(1+V_g)^n}\right) \tag{4}$$

in which $n = 2$ and the thermal conductivity of air k_g, at 20 °C is $0.026\ W\,m^{-1}K^{-1}$. The equation requires a value of k_s for the solid phase and there is a steep dependence of k_s on all forms of porosity at high relative density making k_s relatively difficult to access. Since solid volume fraction $(1 - V_g)$ is calculated from measured density of powdered hydrated paste, the equation requires the conductivity of that material and a putative value can be calculated from the experimental data; a similar approach has been taken to find k_s for hydrated product in a study of fly ash concrete [26]. Using the measured foam conductivities gives k_s between 2.7 and $3.0\ W\,m^{-1}K^{-1}$. For comparison, these lie between the value for vitreous silica and quartz of 1.6 [27] and $8.8\ W\,m^{-1}K^{-1}$ respectively [28]. Using the average experimental value of $k_s = 2.8\ W\,m^{-1}K^{-1}$ it is possible to plot the predicted thermal conductivities as a function of porosity for similar cement foams (Fig. 9).

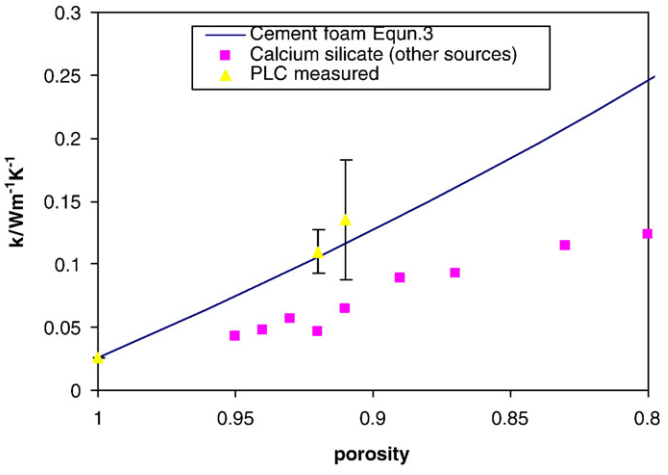

Fig. 9. Thermal conductivity as function of porosity for cement foams (this work). The solid line is Eq. (3). The lower data points are for calcium silicates assembled from other sources as discussed in the script.

Fig. 10 combines the thermal conductivity equation (Eq. (4)) with that for compressive strength (Eq. (3)) to give a figure of merit (FoM) as σ/k:

$$\frac{\sigma}{k} = \frac{0.2\sigma_{fs}(1-V_g)^{\frac{3}{2}}}{k_s(1-A) + k_g A} \tag{5}$$

Using the solid phase thermal conductivity of $k_s = 2.8\ W\,m^{-1}K^{-1}$ and $\sigma_{fs} = 8.9$ MPa this shows how the ratio of strength to conductivity changes with increasing solid phase volume fraction in the region 0 to 0.3. The FoM progressively levels off with decreasing pore volume fraction (V_g) as the benefit of increased strength from reducing the porosity is progressively lost. This curve, for Portland limestone cement foam, provides a baseline. Any intervention, for example addition of toughening agents such as fibres or latex particles or of radiation modifiers such as scatterers or reflectors should position data points above the line.

These foams do not achieve the figures of merit of porous calcium silicate which ranks as one of the best fire resistant, thermal insulating panel materials in terms of apparent conductivity, compressive strength and cost. The main mineral is xonotlite with theoretical density 2700 $kg\,m^{-3}$ and traces of calcite [29] but such boards contain varying amounts of cellulose fibre [30]. In making the following comparisons, absolute densities have been converted to porosity using 2700 $kg\,m^{-3}$ thus over-estimating pore volume, neglecting defective xonotlite crystal structure and the presence of cellulose typically at 8 vol.%. Zheng and Chung [31] obtained a thermal conductivity of $0.046\ W\,m^{-1}K^{-1}$ for a 92% porous material with compressive strength in the region 0.59 MPa giving a FoM of 13 $MKs\,m^{-2}$. Similarly Do et al. [32] report apparent conductivities as low as $0.089\ W\,m^{-1}K^{-1}$ at 20 °C for an 89% porous board. Their data are superimposed on Fig. 9. Measuring thermal conductivity by the hot strip method, similar in principle to the method used here, the data of Wei et al. [33] are also superimposed on Fig. 9. The combined calcium silicate data agree and suggest that the cement foams follow a higher k–volume fraction curve, partly perhaps due to differences in radiative transport, a question that will doubtless receive more attention as the demand for better thermal insulation materials becomes more pressing.

4. Conclusions

A simple method of preparing cementitious foams by stirring powders suspended in water has been established and the formulation

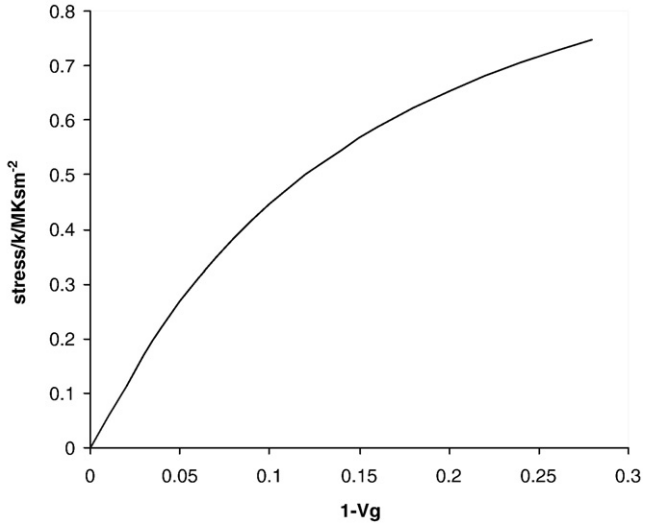

Fig. 10. A Figure of Merit given by crushing strength/thermal conductivity for the cement foams plotted as a function of porosity.

conditions established. The method is transferred from the food industry and uses food additives. At present, the ratio of mechanical strength to thermal conductivity is still too low for these foams to be commercially viable and it would be necessary to protect such foam blocks with a cement skin. The foam is produced by the mechanical incorporation of air and stabilised by a mixture of methyl cellulose and iota carageenan gum. Experimental work established the composition ranges for high porosity (>90%) foam formation. The organic constituent iCG contributes to foam stability by reducing foam drainage but does not participate in foaming and was used at ~0.13 wt.% based on cement powder. MC is essential for foam formation and was also used at 0.13 wt.%. In order to maintain a 90% porosity level or more a high w/c ratio should be used. To attain >85% porosity in the plaster foams a water/gypsum ratio of 1.6 was needed.

It was thought that dispersed glass fibres would reinforce the structure but in practice, failure of the whole structure occurred at once because the fibres transmitted the load throughout thus preventing steady, progressive collapse. Fibre addition does not therefore improve compressive strength but it does allow the foam to sustain increasing load post fracture. An overall figure of merit was used to show how both strength and thermal conductivity change with porosity. This showed that the benefit of increased strength from reducing the porosity is progressively lost and, because it is constructed for unmodified cement powder provides a baseline upon which to compare interventions to increase strength or decrease apparent conductivity.

Acknowledgements

The authors are grateful to Linda Bellecom-Allen (Dow Methocel Food Group Europe) for advice and to Dr. Adam Wojcik (UCL) for use of the mechanical testing equipment.

References

[1] D.M. Liu, Fabrication of hydroxyapatite ceramic with controlled porosity, J. Mater. Sci., Mater. Med. 8 (1997) 227–232.
[2] A.M. Williams, C.P. Garner, J.G.P. Binner, Proc. Inst. Mech. Engnrs, D, J. Auto Eng. 222 (2008) 2235–2247.
[3] C.M.S. Ranito, F.A.C. Oliveira, J.P. Borges, Hydroxyapatite foams for bone replacement, Bioceramics 17, Key Eng. Mat. 284–286 (2005) 341–344.
[4] P. Colombo, M. Griffoni, M. Modesti, Ceramic foams from a preceramic polymer and polyurethanes, J. Sol–gel Sci. Technol. 13 (1998) 195–199.
[5] S.J. Powell, J.R.G. Evans, The structure of ceramic foams prepared from polyurethane ceramic suspensions, Mater. & Manuf. Proc. 10 (1995) 757–771.
[6] C. Tuck, J.R.G. Evans, Porous ceramics prepared from protein foams, J. Mater. Sci. Lett. 18 (1999) 1003–1005.
[7] P.G. Collishaw, J.R.G. Evans, An assessment of expressions for calculating the apparent thermal conductivity of cellular materials, J. Mater. Sci. 29 (1994) 2261–2273.
[8] K. Raed, U. Gross, Review on gas thermal conductivity in porous materials and Knudsen effect, in: J.R. Koenig, H. Ban (Eds.), Joint 29th Int. Thermal. Cond. Conf./17th Int. Thermal Exp. Symp. Birm. Al. June 2007, Univ. Alabama, 2007, pp. 356–373.
[9] T.D. Tonyan, L.J. Gibson, Structure and mechanics of cement foams, J. Mater. Sci. 27 (1992) 6371–6378.
[10] G.N. Karam, T.D. Tonyan, Fractal morphology of cement foams, Mater. Lett. 16 (1993) 278–280.
[11] H.N. Atahan, C. Carlos, S. Chae, P.J.M. Monteiro, J. Bastacky, The morphology of entrained air voids in hardened cement paste generated with different anionic surfactants, Cem. & Conc. Comp. 30 (2008) 566–575.
[12] L. Verdolotti, E. Di Maio, M. Lavorgna, S. Iannace, L. Nicolais, Polyurethane-cement based foams: characterization and potential uses, J. Appl. Polym. Sci. 107 (2008) 1–8.
[13] D. Meyer, J.G.M. van Mier, Influence of different PVA fibres on the crack behaviour of foamed cement paste, Proc. & Monogr. in Eng., Water and Earth Sci. 1–3 (2007) 1359–1365.
[14] T.D. Tonyan, L.J. Gibson, Strengthening of cement foams, J. Mater. Sci. 27 (1992) 6379–6386.
[15] G. Li, V.D. Muthyala, A cement based syntactic foam, Mater. Sci. Eng A 478 (2008) 77–86.
[16] EN993-15 Methods of test for dense shaped refractory products; Determination of thermal conductivity by the hot-wire parallel method, Euro. Committee for Standardisation, Brussels, 2005.
[17] H. Minard, S. Garrault, L. Regnaud, A. Nonat, Mechanisms and parameters controlling the tricalcium aluminate reactivity in the presence of gypsum, Cem. Conc. Res. 37 (2007) 1418–1426.
[18] J. Pourchez, P. Grosseau, B. Ruot, Current understanding of cellulose ethers' impact on the hydration of C_3A and C_3A-sulphate systems, Cem Conc. Res. CEMCON-03911 39 (2009) 664–669.
[19] H.X. Peng, Z. Fan, J.R.G. Evans, J.J.C. Busfield, Microstructure of ceramic foams, J. Euro. Ceram. Soc. 20 (2000) 807–813.
[20] J. Hill, J.H. Sharp, The mineralogy and microstructure of three composite cements with high replacement levels, Cement and Conc. Res. 24 (2002) 191–199.
[21] N. Voglis, G. Kakali, E. Chaniotakis, S. Tsivilis, Portland-limestone cements; their properties and hydration compared to those of composite cements, Cem. Concr. Compos. 27 (2005) 191–196.
[22] G. Barluenga, F. Hernández-Olivares, Cracking control of concretes modified with short AR-glass fibers at early age. Experimental results on standard concrete and SCC, Cem. Conc. Res. 37 (2007) 1624–1638.
[23] L.J. Gibson, M. Ashby, Cellular solids: Structure and properties, Cambridge University Press, UK, Edn. 2nd, pp. 175–231.
[24] R. Wulf, G. Barth, U. Gross, Intercomparison of insulation thermal conductivities measured by various methods, Int. J. Thermophys. 28 (2007) 1679–1692.
[25] L.C.K. Carwile, H.J. Hoge, Tech. Reprot 66–27-PR Thermal conductivity of polystyrene: Selected values, Pioneering Res. Divn. U.S.Army Natick Labs. Natick Mass. 01760, April 1966, p. 5.
[26] P. Choktaweekarn, W. Saengsoy, S. Tangtermsirikul, A model for predicting thermal conductivity of concrete, Mag. Conc. Res. 61 (2009) 271–280.
[27] G.W.C. Kaye, T.H. Laby, Tables of physical constants, 16th ed. Longman, Essex, UK p. 91.
[28] R.C. Weast (Ed.), Handbook of Chemistry and Physics, 55th Ed, CRC Press, Ohio, USA, 1975, p. E5.
[29] A. Hamilton, C. Hall, Physicochemical characterization of a hydrated calcium silicate board material, J. Building Phys. 29 (2005) 9–18.
[30] A. Hamilton, C. Hall, A note on the density of a calcium silicate hydrate board material, J. Building Phys. 31 (2007) 69–71.
[31] Q. Zheng, D.D.L. Chung, Microporous calcium silicate thermal insulator, Mat. Sci. Technol. 6 (1990) 666–669.
[32] C.T. Do, D.P. Bentz, P.E. Stutzman, Microstructure and thermal conductivity of hydrated calcium silicate board materials, J. Building Phys. 31 (2007) 55–67.
[33] G. Wei, X. Zhang, F. Yu, Thermal conductivity measurements on xonotlite-type calcium silicate by the hot-strip method, J. Univ. Sci & Technol. Beijing 15 (2008) 791–795.